A Ratiometric Catalog of Protein Isoform Shifts in the Cardiac Fetal Gene Program

[1]Yu Han, [1]Sara A. Wennersten, [1]Boomathi P. Pandi, [1]Dominic C. M. Ng, [1]Edward Lau, [1,2,3]Maggie P. Y. Lam

1. Department of Medicine
2. Department of Biochemistry and Molecular Genetics
3. Consortium for Fibrosis Research and Translation
University of Colorado School of Medicine
Aurora, CO 80045, USA

Correspondence: Maggie Lam, PhD. Email: maggie.lam@cuanschutz.edu

Abstract

The fetal genetic program orchestrates cardiac development and the re-expression of fetal genes is thought to underlie cardiac disease and adaptation. Here, a proteomics ratio test using mass spectrometry is applied to find protein isoforms with statistically significant usage differences in the fetal vs. postnatal mouse heart. Changes in isoform usage ratios are pervasive at the protein level, with 104 significant events observed, including 88 paralog-derived isoform switching events and 16 splicing-derived isoform switching events between fetal and postnatal hearts. The ratiometric proteomic comparisons rediscovered hallmark fetal gene signatures including a postnatal switch from fetal β (MYH7) toward α (MYH6) myosin heavy chains and from slow skeletal muscle (TNNI1) toward cardiac (TNNI3) troponin I. Altered usages in metabolic proteins are prominent, including a platelet to muscle phosphofructokinase (PFKP - PFKM), enolase 1 to 3 (ENO1 - ENO3), and alternative splicing of pyruvate kinase M2 toward M1 (PKM2 - PKM1) isoforms in glycolysis. The data also revealed a parallel change in mitochondrial proteins in cardiac development, suggesting the shift toward aerobic respiration involves also a remodeling of the mitochondrial protein isoform proportion. Finally, a number of glycolytic protein isoforms revert toward their fetal forms in adult hearts under pathological cardiac hypertrophy, suggesting their functional roles in adaptive or maladaptive response, but this reversal is partial. In summary, this work presents a catalog of ratiometric protein markers of the fetal genetic program of the mouse heart, including previously unreported splice isoform markers.

Introduction

Gene expression profiles in mammalian tissues can differ dramatically between fetal and postnatal stages in response to changing energetic and physiological environments, e.g., human fetal hemoglobin (HbF) in utero vs. adult hemoglobin (HbA) after birth. In the case of the myocardium, the fetal heart inhabits a low-oxygen environment and prefers carbohydrate substrates. Upon birth, multiple metabolic and contractile fetal genes shift in expression, which underlies a striking change in phenotypes from the fetal toward the postnatal heart that utilizes fatty acid oxidation as fuel. Interestingly, in failing and pathological hearts, a reversal toward fetal genes is often observed in conjunction with pathologies, documented to be driven by the re-activation of several known developmental transcription factors such as NFAT and MEF2 (Dirkx et al., 2013; Rajabi et al., 2007). While it remains debated whether the return to the fetal genetic program in pathological hearts is primarily adaptive (Rajabi et al., 2007; Taegtmeyer et al., 2010) or maladaptive (Dirkx et al., 2013), the fetal genetic program is a topic of interest in cardiobiology as it pertains to understanding cardiac development as well as pathological cardiac remodeling.

We aimed to discover the extent of fetal genes in the heart at the protein level, which would be important for understanding physiological changes during development and disease. Changes in fetal and postnatal genes often involve the differential usage of *gene isoforms*, a broadly defined term that encompasses members of a gene family that share significant sequence homology, overlapping functions, and regulatory modalities. Isoforms can originate from two distinct genes that have diversified from past

gene duplication events, i.e., paralogs; as well as from variants of the same gene due to alternative splicing patterns, which are known to alter significantly during cardiac development (Wang et al., 2016). Importantly, the *ratio* between two gene products is frequently the determinant of functional phenotypes rather than the individual expression level of either gene (Bergeron et al., 2010; Gelens et al., 2018; Warren et al., 2019; Zannoni et al., 2013). Thus, the ratiometric changes of isoform pairs present an important dimension to understanding fetal gene usage and its implication in the phenotypic changes between fetal and adult hearts.

Transcript measurements have identified many isoform usage differences across cardiac development (D'Antonio et al., 2022; DeLaughter et al., 2016), but protein translation and levels cannot be predicted from mRNA with certainty (Gygi et al., 1999; Payne, 2015; Srivastava et al., 2022; Yang et al., 2020). Defining the proteomic impact of isoform shifts is therefore needed to understand the functional consequence of fetal gene expression. At the protein level, fetal genes are conventionally conceptualized through comparing the levels of functionally related proteins in protein families using immunoblots or histochemistry techniques, for example, the reciprocal intensity of α vs. β myosin heavy chains (Franco et al., 1998; Reiser et al., 2001). Although immunobiological techniques can reveal the relative fold-changes of each isoform, further calibration may be needed to quantify the proportion of proteins, such as in cases of differential affinities of antibodies against different targets or epitopes. Without considering the absolute abundance of each isoform, a large fold-change may be reported due to a minor isoform of very low abundance being in the denominator of the ratio calculation. On the other hand, large-scale mass spectrometry experiments can be used to quantify the relative levels of thousands of proteins in an experiment, and have been successfully applied to profiling the proteomes of fetal hearts (Lu et al., 2014). Nevertheless, most proteomics studies concern only the comparison of expression of the same proteins across conditions but do not explicitly test for ratios across genes/proteins. To our knowledge, a clear catalog of the major detectable protein isoform changes in the fetal genetic program remains elusive, and protein-level data of splicing-derived protein isoforms (hereafter referred to as "spliceoforms") are in particular scarce.

Results and Discussion

To discover the extent of fetal heart genes at the protein level, we applied a proteomic ratio test, using the multiplexing ability of tandem mass tag (TMT) isotope label-based quantitation in MS2 scans in conjunction with label-free intensity-based absolute quantification (iBAQ) in MS1 scans to compare the absolute expression of two protein isoforms across multiple samples. We implemented a simple workflow that combines MS1 and MS2 information to compare the protein abundance ratios of gene paralogs in fetal vs. postnatal hearts as illustrated in **Figure 1A** (see Methods for details). TMT-labeled mass spectrometry data, measured at the MS2 level, readily distinguished fetal and postnatal protein expression profiles in PC1 and PC2 (**Figure 1B**). On a per-protein level, we quantified the relative fetal/postnatal abundance of 3,913 canonical UniProt proteins, among which 1,991 proteins were differentially expressed at FDR-adjusted limma p value < 0.01 (**Supplemental Figure S1A**). As expected, differentially expressed proteins are enriched in processes important for cardiac development including cell cycle, mRNA splicing, mitochondrial translation, and complex I biogenesis terms (gene set enrichment analysis GSEA FDR adjusted q-value < 0.01), suggesting our mass spectrometry data were able to capture rich age-specific differences in proteomic landscape of the fetal and postnatal hearts. (**Supplemental Figure S1B**).

Calculating the shifts in paralog usage would require comparison of one protein to another. Hence in the workflow we next calculated the protein intensity-based absolute quantification (iBAQ) values from MS1 label-free quantification (LFQ) information from each protein and then used the proportional abundance of the MS2 TMT channels to allocate protein abundance across the individual samples (**Figure 1A**; see methods). The overall MS1-MS2 combined iBAQ values spanned over 5 orders of magnitude (**Figure 1C**).

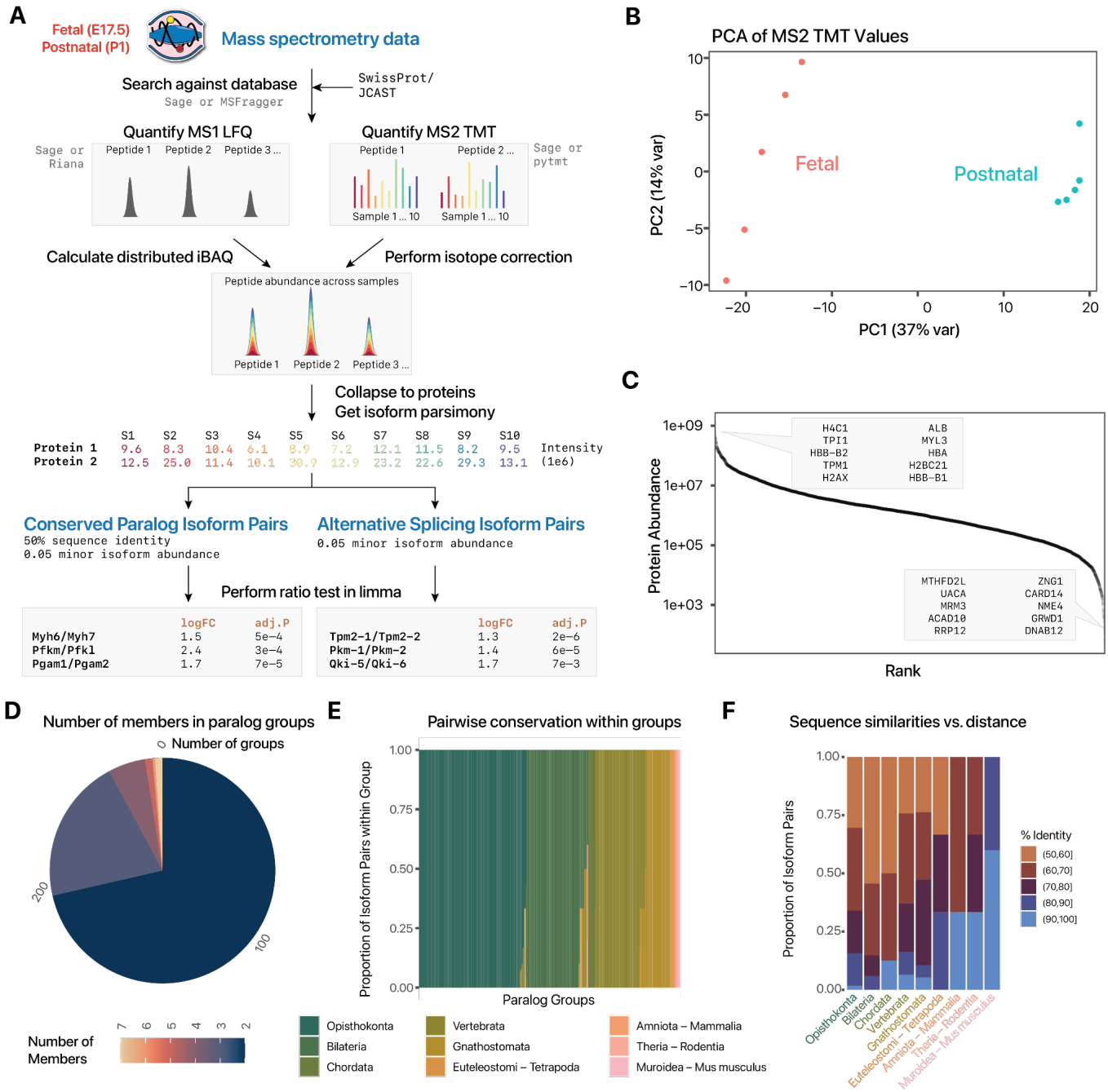

Figure 1. Experimental and analytical workflow of isoform usage tests. **A:** Mass spectrometry data were generated from fetal (E17.5) and postnatal (P1) mouse hearts (n=5 each). Label-free MS1 and TMT MS2 intensities were extracted from the data, which contained information on across-peptide intensities and within-peptide intensities across experiments, respectively. We performed protein parsimony grouping, isotope correction, and calculated the ratios between pairs of paralogous gene isoform proteins and between alternative splicing isoform proteins. **B.** Relative peptide abundance from TMT intensities shows clear segregation between fetal and postnatal heart samples. **C.** Protein abundance values spanned over 5 orders of magnitude. The 10 most and least abundant proteins are shown in the boxes. **D.** Pie chart showing the proportion of paralog groups with 2 (blue) to 7 (pink) group members. **E.** Sorted proportional bar charts showing the evolutionary conservation of all paralog pairs within each of the paralog groups from the most conserved (across Opisthokonta) to the least (Muroidea to Mus). **F.** Proportional bar charts showing the binned average sequence homology among all paralog pairs within each conservation

distance category. Only paralog pairs with an average of 50% average % identity are compared. Open bracket "(": non-inclusive interval; closed bracket "]": inclusive interval.

We retrieved conserved gene paralog pairs using Ensembl genome annotation with additional filtering for at least 50% sequence homology, then further grouped the protein pairs into non-overlapping paralog groups. In total, we identified 280 groups of paralogs among quantified proteins ranging from 2 to 7 protein members each (median [IQR]: 2.0 [2.0 – 3.0] members) (**Figure 1D**), consisting of 545 quantifiable pairwise paralog relationships and median of 66.7% [59.8% – 76.7%] sequence identity (**Figure 1E**), among which 97.8% of paralog pairs are conserved across mammals (**Figure 1F**). From these, we compared the differential abundance ratios of the pairs of paralogs between fetal and postnatal mouse hearts, out of which 154 pairs were significantly different at limma adjusted $P < 0.01$ (**Figure 2A**) while having a minor isoform fraction of at least 5% on average of all samples. We then prioritized 88 pairs of paralog proteins with close sequence homology that show absolute log2 fold-changes of 0.5 or more in fetal/postnatal hearts and are conserved at least across Mammalia. These prioritized paralogous proteins belong to 73 distinct isoform groups. The top 25 protein pairs are shown in **Table 1** and notable changes are highlighted in the sections below.

Paralog Pair	logFC	adj.P.Val	Paralog 1 Protein Name	Paralog 2 Protein Name	MIF	Conservation
Myh6/Myh7	-4.292	4.08E-08	Myosin-6 (Myosin heavy chain 6) (Myosin heavy chain, cardiac muscle alpha isoform) (MyHC-alpha)	Myosin-7 (Myosin heavy chain 7) (Myosin heavy chain slow isoform) (MyHC-slow) (Myosin heavy chain, cardiac muscle beta isoform) (MyHC-beta)	0.419	Opisthokonta
Hmgcs2/Hmgcs1	-3.012	2.95E-07	Hydroxymethylglutaryl-CoA synthase, mitochondrial (HMG-CoA synthase) (EC 2.3.3.10) (3-hydroxy-3-methylglutaryl coenzyme A synthase)	Hydroxymethylglutaryl-CoA synthase, cytoplasmic (HMG-CoA synthase) (EC 2.3.3.10) (3-hydroxy-3-methylglutaryl coenzyme A synthase)	0.082	Gnathostomata
Myl4/Myl3	2.558	3.42E-05	Myosin light chain 4 (MLC1EMB) (Myosin light chain 1, atrial/fetal isoform) (MLC1A)	Myosin light chain 3 (Myosin alkali light chain 1, ventricular/slow skeletal muscle isoform) (Myosin light chain 1, slow-twitch muscle B/ventricular isoform) (MLC1SB)	0.152	Gnathostomata
Slc2a1/Slc2a4	2.519	8.08E-08	Solute carrier family 2, facilitated glucose transporter member 1 (Glucose transporter type 1, erythrocyte/brain) (GLUT-1) (GT1)	Solute carrier family 2, facilitated glucose transporter member 4 (GT2) (Glucose transporter type 4, insulin-responsive) (GLUT-4)	0.496	Opisthokonta
Pgam1/Pgam2	2.184	1.03E-08	Phosphoglycerate mutase 1 (EC 5.4.2.11) (EC 5.4.2.4) (BPG-dependent PGAM 1) (Phosphoglycerate mutase isozyme B) (PGAM-B)	Phosphoglycerate mutase 2 (EC 5.4.2.11) (EC 5.4.2.4) (BPG-dependent PGAM 2) (Muscle-specific phosphoglycerate mutase) (Phosphoglycerate mutase isozyme M) (PGAM-M)	0.256	Gnathostomata
Tnni3/Tnni1	-2.07	8.26E-08	Troponin I, cardiac muscle (Cardiac troponin I)	Troponin I, slow skeletal muscle (Troponin I, slow-twitch isoform)	0.469	Chordata
Ckb/Ckmt2	2.05	6.1E-08	Creatine kinase B-type (EC 2.7.3.2) (B-CK) (Creatine kinase B chain) (Creatine phosphokinase B-type) (CPK-B)	Creatine kinase S-type, mitochondrial (EC 2.7.3.2) (Basic-type mitochondrial creatine kinase) (Mib-CK) (Sarcomeric mitochondrial creatine kinase) (S-MtCK)	0.13	Bilateria

Eno1/Eno3	2.009	5.38E-08	Alpha-enolase (EC 4.2.1.11) (2-phospho-D-glycerate hydro-lyase) (Enolase 1) (Non-neural enolase) (NNE)	Beta-enolase (EC 4.2.1.11) (2-phospho-D-glycerate hydro-lyase) (Enolase 3) (Muscle-specific enolase) (MSE) (Skeletal muscle enolase)	0.466	Vertebrata
Pfkm/Pfkl	-1.683	4.64E-09	ATP-dependent 6-phosphofructokinase, muscle type (ATP-PFK) (PFK-M) (EC 2.7.1.11) (6-phosphofructokinase type A) (Phosphofructo-1-kinase isozyme A) (PFK-A) (Phosphohexokinase)	ATP-dependent 6-phosphofructokinase, liver type (ATP-PFK) (PFK-L) (EC 2.7.1.11) (6-phosphofructokinase type B) (Phosphofructo-1-kinase isozyme B) (PFK-B) (Phosphohexokinase)	0.072	Opisthokonta
Rdh11/Rdh12	1.453	5.08E-04	Retinol dehydrogenase 11 (EC 1.1.1.300) (Androgen-regulated short-chain dehydrogenase/reductase 1) (Cell line MC/9.IL4-derived protein 1) (M42C60) (Prostate short-chain dehydrogenase/reductase 1) (Retinal reductase 1) (RalR1) (Short-chain aldehyde dehydrogenase) (SCALD)	Retinol dehydrogenase 12 (EC 1.1.1.300)	0.253	Opisthokonta
Pzp/A2m	-1.447	7.81E-07	Pregnancy zone protein (Alpha-2-macroglobulin) (Alpha-2-M) [Cleaved into: Alpha-2-macroglobulin 165 kDa subunit; Alpha-2-macroglobulin 35 kDa subunit]	Pregnancy zone protein (Alpha-2-macroglobulin) (Alpha-2-M) [Cleaved into: Alpha-2-macroglobulin 165 kDa subunit; Alpha-2-macroglobulin 35 kDa subunit]	0.487	Bilateria
Pzp/A2m	-1.447	7.81E-07	Pregnancy zone protein (Alpha-2-macroglobulin) (Alpha-2-M) [Cleaved into: Alpha-2-macroglobulin 165 kDa subunit; Alpha-2-macroglobulin 35 kDa subunit]	Alpha-2-macroglobulin-P (Alpha-2-macroglobulin)	0.487	Bilateria
Pfkm/Pfkp	-1.446	8.24E-08	ATP-dependent 6-phosphofructokinase, muscle type (ATP-PFK) (PFK-M) (EC 2.7.1.11) (6-phosphofructokinase type A) (Phosphofructo-1-kinase isozyme A) (PFK-A) (Phosphohexokinase)	ATP-dependent 6-phosphofructokinase, platelet type (ATP-PFK) (PFK-P) (EC 2.7.1.11) (6-phosphofructokinase type C) (Phosphofructo-1-kinase isozyme C) (PFK-C) (Phosphohexokinase)	0.279	Opisthokonta
Fbn2/Fbn1	1.42	1.05E-07	Fibrillin-2 [Cleaved into: Placensin]	Fibrillin-1 [Cleaved into: Asprosin]	0.183	Chordata
Myh11/Myh10	-1.377	7.12E-06	Myosin-11 (Myosin heavy chain 11) (Myosin heavy chain, smooth muscle isoform) (SMMHC)	Myosin-10 (Cellular myosin heavy chain, type B) (Myosin heavy chain 10) (Myosin heavy chain, non-muscle IIb) (Non-muscle myosin heavy chain B) (NMMHC-B) (Non-muscle myosin heavy chain IIb) (NMMHC II-b) (NMMHC-IIB)	0.303	Opisthokonta
Ppia/Ppif	1.313	9.91E-07	Peptidyl-prolyl cis-trans isomerase A (PPIase A) (EC 5.2.1.8) (Cyclophilin A) (Cyclosporin A-binding protein) (Rotamase A) (SP18) [Cleaved into: Peptidyl-prolyl cis-trans isomerase A, N-terminally processed]	Peptidyl-prolyl cis-trans isomerase F, mitochondrial (PPIase F) (EC 5.2.1.8) (Cyclophilin D) (CyP-D) (CypD) (Cyclophilin F) (Rotamase F)	0.102	Opisthokonta
Pdk3/Pdk2	1.272	3.49E-07	[Pyruvate dehydrogenase (acetyl-transferring)] kinase isozyme 3, mitochondrial (EC 2.7.11.2) (Pyruvate dehydrogenase kinase isoform 3)	[Pyruvate dehydrogenase (acetyl-transferring)] kinase isozyme 2, mitochondrial (EC 2.7.11.2) (Pyruvate dehydrogenase kinase isoform 2) (PDH kinase 2)	0.219	Vertebrata
Ppa2/Ppa1	-1.271	2.01E-06	Inorganic pyrophosphatase 2, mitochondrial (EC 3.6.1.1) (Pyrophosphate phospho-hydrolase 2) (PPase 2)	Inorganic pyrophosphatase (EC 3.6.1.1) (Pyrophosphate phospho-hydrolase) (PPase)	0.443	Vertebrata

Septin6/Septin8	1.246	1.02E-04	Septin-6	Septin-8	0.075	Opisthokonta
Eif4ebp2/Eif4ebp1	-1.198	2.2E-04	Eukaryotic translation initiation factor 4E-binding protein 2 (4E-BP2) (eIF4E-binding protein 2) (Phosphorylated heat- and acid-stable protein regulated by insulin 2) (PHAS-II)	Eukaryotic translation initiation factor 4E-binding protein 1 (4E-BP1) (eIF4E-binding protein 1) (Phosphorylated heat- and acid-stable protein regulated by insulin 1) (PHAS-I)	0.278	Bilateria
Eef1a1/Eef1a2	1.18	5.33E-07	Elongation factor 1-alpha 1 (EF-1-alpha-1) (EC 3.6.5.-) (Elongation factor Tu) (EF-Tu) (Eukaryotic elongation factor 1 A-1) (eEF1A-1)	Elongation factor 1-alpha 2 (EF-1-alpha-2) (Eukaryotic elongation factor 1 A-2) (eEF1A-2) (Statin-S1)	0.195	Vertebrata
Ckm/Ckmt2	1.133	1.01E-05	Creatine kinase M-type (EC 2.7.3.2) (Creatine kinase M chain) (Creatine phosphokinase M-type) (CPK-M) (M-CK)	Creatine kinase S-type, mitochondrial (EC 2.7.3.2) (Basic-type mitochondrial creatine kinase) (Mib-CK) (Sarcomeric mitochondrial creatine kinase) (S-MtCK)	0.13	Bilateria
Dynll1/Dynll2	1.086	3.71E-06	Dynein light chain 1, cytoplasmic (8 kDa dynein light chain) (DLC8) (Dynein light chain LC8-type 1) (Protein inhibitor of neuronal nitric oxide synthase) (PIN) (mPIN)	Dynein light chain 2, cytoplasmic (8 kDa dynein light chain b) (DLC8) (DLC8b) (Dynein light chain LC8-type 2)	0.411	Chordata
Tuba4a/Tuba8	-1.065	1.4E-06	Tubulin alpha-4A chain (EC 3.6.5.-) (Alpha-tubulin 4) (Alpha-tubulin isotype M-alpha-4) (Tubulin alpha-4 chain)	Tubulin alpha-8 chain (EC 3.6.5.-) (Alpha-tubulin 8) [Cleaved into: Dephenylalaninated tubulin alpha-8 chain]	0.164	Opisthokonta
Car1/Car2	-1.03	3.03E-04	Carbonic anhydrase 1 (EC 4.2.1.1) (Carbonate dehydratase I) (Carbonic anhydrase I) (CA-I) (Cyanamide hydratase CA1) (EC 4.2.1.69)	Carbonic anhydrase 2 (EC 4.2.1.1) (Carbonate dehydratase II) (Carbonic anhydrase II) (CA-II) (Cyanamide hydratase CA2) (EC 4.2.1.69)	0.102	Bilateria

Table 1: Top 25 conserved paralogous proteins with significant shifts in isoform usage between fetal vs. postnatal hearts, ranked by absolute log2 fold-changes (logFC) in protein abundance ratios (fetal/postnatal). MIF: minor isoform fraction.

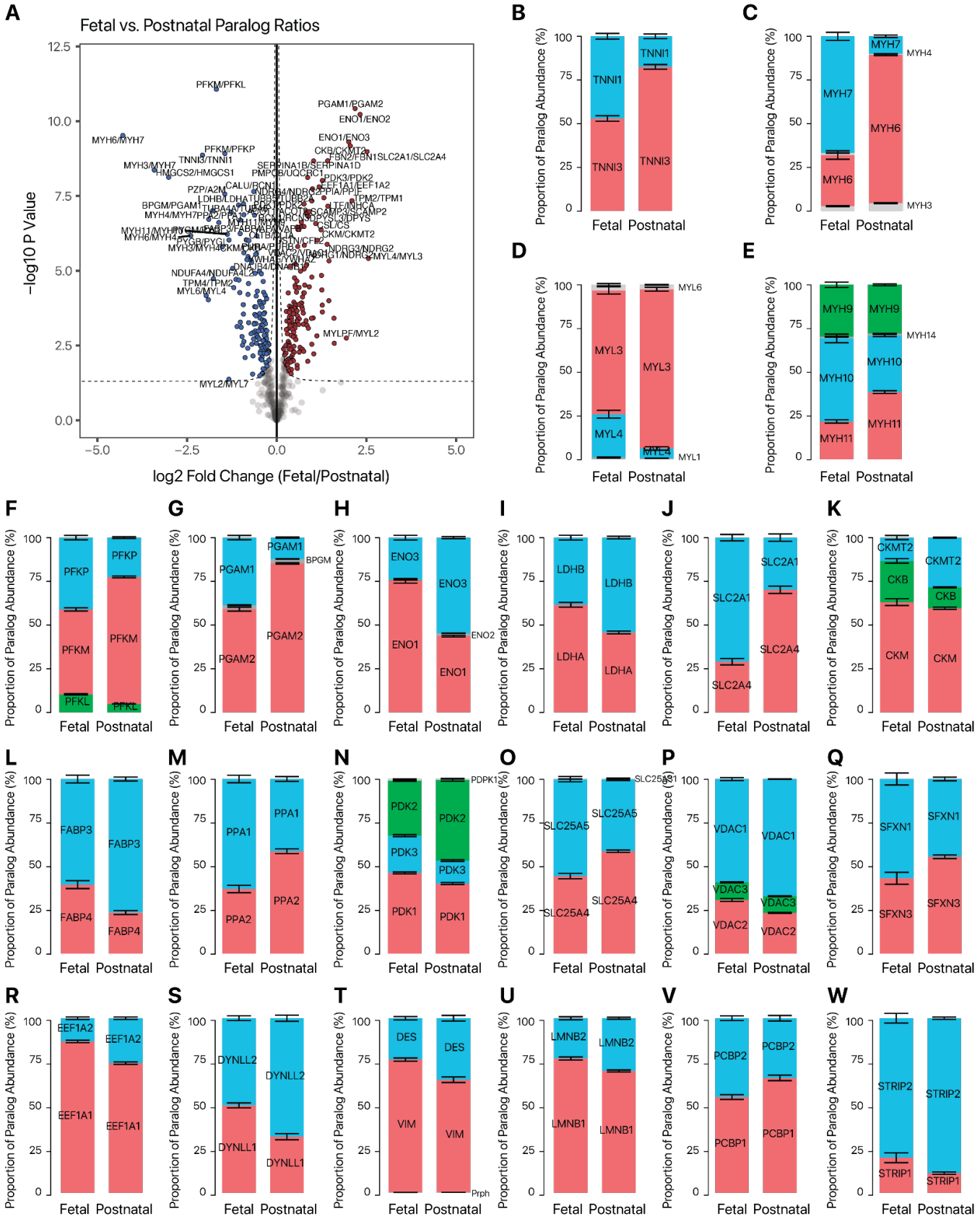

Figure 2. Protein isoform shift in fetal vs. postnatal hearts. **A.** Volcano plot showing the log2 fold-change (x-axis) vs. –log10 P value (y-axis) of compared paralog pairs (n=5 for fetal and postnatal hearts each). **B–E**. Bar charts showing the proportion from 0 to 100% of **B.** TNN1/TNN3 **C.** MYH6/MYH7 **D.** MYL3/MYL4

and **E.** MYH10/MYH11 within their paralog groups in fetal and postnatal hearts, showing a shift in isoform usage among hallmark fetal genes. Error bars: s.e.m. of cumulative proportion. **F–W.** Proportional bar charts showing significant shifts in isoform ratios among selected **F–K.** glycolysis proteins; **L–Q.** mitochondrial proteins; and **R–W.** structural and signaling proteins. Error bars: s.e.m. of cumulative proportion; n=5 fetal and hypertrophic hearts each. Selected isoform pairs are shown with limma adjusted $P < 0.01$; average minor isoform fraction ≥ 0.05; sequence identity > 50%, and conserved across mammals.

Shifts in paralog protein ratios in fetal vs. postnatal hearts

The isoforms with differential usage recapitulate previously known features of the fetal genetic program, and can be grouped into major functional groups:

i. Among contractile proteins, the use of the β myosin heavy chain is a well-established hallmark of the fetal genetic program (Reiser et al., 2001). Consistently, we observed a prominent ~20-fold reciprocal shift from β myosin heavy chain (MYH7) toward α (MYH6) myosin heavy chains from fetal to postnatal hearts. In fetal hearts, MYH7 to MYH6 ratio is >2 to 1, whereas in postnatal hearts, MYH6 is >8 fold higher than MYH7 (**Figure 2B**). Secondly, a developmental stage-specific expression of fetal troponin I is another well-established hallmark in fetal development (Bhavsar et al., 1991). Consistently, we recapitulated a >4-fold relative shift from slow skeletal muscle type troponin I (TNNI1) toward the adult cardiac type (TNNI3), where they are expressed ~1:1 in fetal hearts but TNNI3 is >4-fold higher in postnatal hearts (Figure 2C). Other changes in contractile proteins include the known difference in ventricular vs. fetal myosin light chains. The data recapitulated a >5-fold further enrichment of the ventricular MYL3 over fetal/essential MYL4 in postnatal hearts, where MYL3 is already expressed at ~3-fold higher in the fetal heart than MYL4, but is dramatically enriched to ~16-fold higher in postnatal heart (**Figure 2D**). Another contractile protein usage difference concerns a 2.6-fold shift from the non-muscle myosin polypeptide MYH10 toward the smooth muscle myosin heavy polypeptide MYH11, where MYH10 is 2-fold higher than MYH11 in fetal heart, but lower in postnatal hearts (**Figure 2E**).

ii. Prominent changes are also seen among proteins that function in glycolysis. The glycolytic enzyme, phosphofructokinase, which exists as 3 isoforms: PFKM (muscle); PFKP (platelet); and PFKL (liver), sees an expansion of the muscle isoform from fetal heart (49%) to postnatal heart (73%) coupled to the contraction of liver (10% to 5%) and platelet (41% to 23%) isoforms (**Figure 2F**), consistent with isozyme biochemical activity assays (Thrasher et al., 1981). Another glycolytic enzyme, phosphoglycerate mutase (PGAM1/2), the proportion of the skeletal muscle and myocardial enriched type-M isoform (PGAM2) went up from 59% to 85% of the paralog group between fetal to postnatal hearts, whereas the proportion of the type-B isoform PGAM1 decreased from 39% to 11% (**Figure 2G**).In fetal hearts, enolase 1 (ENO1) is the predominant isoform, amounting to 75% of abundance within the paralog group, but decreases to 43% in postnatal heart (**Figure 2H**). This is coupled with an increase from 24% to 55% of the striated muscle isoform ENO3, a ~4-fold switch in ENO1/ENO3 ratios. In fetal hearts, lactate dehydrogenase H vs. M subunits (LDHA)/(LDHB) existed at 61%/38% ratio, which changed to 45%/54% in postnatal hearts, a 1.9-fold switch (**Figure 1I**). This shift is consistent with the known enrichment of lactate dehydrogenase complexes containing the H subunit LDHB in the heart and its preference for conversion of lactate toward pyruvate in oxidative metabolism environment, as opposed to the preference of the M subunit LDHA to favor lactate production from pyruvate in glycolytic tissues (Read et al., 2001).

Related to glycolysis, fetal hearts express more basal glucose transporter GLUT1 (SLC2A1) than insulin-sensitive GLUT4 (SLC2A4) in a 71%/29% ratio, but roughly opposite proportion in postnatal hearts (30%/70% ratio) (**Figure 2J**). A transition from GLUT1 to GLUT4 in neonatal development is known in the heart and in brown fat of rats (Castelló et al., 1994), whereas prior work using transcript data whereas both GLUT1 and GLUT4 are more highly expressed in adult than fetal human hearts (Taegtmeyer et al., 2010). Finally, there is a decrease in proportion of non-muscle type cytosolic creatine kinase (CKB), but a reciprocal increase in the proportion of mitochondrial matrix

creatine kinase (CKMT2) (**Figure 2K**).

iii. These changes are coupled to prominent changes in mitochondrial proteins, some of which have not been typically associated as part of the fetal genetic program. These include a ~2-fold further enrichment of FABP3 over FABP4 (from 61%/39% ratios to 76%/24% ratios) in postnatal hearts (**Figure 2L**), which was also observed in single-cell transcripts in developing mouse hearts from E9.5 to P21 (DeLaughter et al., 2016). In conjunction, we see a 2.3-fold reciprocal swing from PPA1 to PPA2 (**Figure 2M**), and a switch from pyruvate dehydrogenase 1 and 3 (PDK1/PDK3) toward PDK2 as the major pyruvate dehydrogenase kinase isozyme (**Figure 2N**).

At the same time, the skeletal muscle form of ADP/ATP carrier ANT1 (SLC25A4) replaces the fibroblast form (SLC25A5) ANT2 as the prevalent ADP/ATP carrier (**Figure 2O).** A further increase of the ratio of VDAC1 to VDAC2 ratio in the mitochondrial voltage-dependent anion channel is observed (**Figure 2P**). The complex function and regulation of VDAC isoforms remains to be elucidated (Baines et al., 2007) but VDAC1 may promote (Anflous et al., 2001) and VDAC2 may inhibit apoptosis (Cheng et al., 2003); hence a change in VDAC1/VDAC2 ratio could affect mitochondrial physiology. Finally, there is a shift of sideroflexin, a mitochondrial membrane transporter involved in iron transport, from the ubiquitous SFXN1 isoform toward the neuron-enriched SFXN3 isoform (**Figure 2Q**).

During fetal cardiac development and toward birth, there is a metabolic shift from glycolytic toward aerobic metabolism in the heart which involves mitochondrial biogenesis as well as other remodeling (Zhao et al., 2019). The observations here suggest that this remodeling involves changes in isoform usage in mitochondrial proteins in parallel to changes in glycolytic proteins.

iv. Other changes related to gene regulation and structural proteins include a switch in translation elongation factors EEF1A1 and EFF1A2 (**Figure 2R**), where the former is 6.5-fold higher in fetal hearts but about 3-fold higher in postnatal hearts. There is a switch from DYNLL1 toward DYNLL2 as the major isoform in postnatal hearts (50%/50% in fetal hearts, vs. 32%/68% in postnatal hearts) (**Figure 2S**), and finally, a subtle switch of vimentin (VIM)/desmin (DES) ratios (76%/24% to 64%/35%) (**Figure 2T**), a slight increase in Lamin B2 (LMNB2) vs B1 (LMNB1) (**Figure 2U**), PCBP1 (**Figure 2V**), and STRIP2 (**Figure 2W**).

<u>Shifts in protein spliceoform ratios in fetal vs. postnatal hearts</u>

We next examined whether splicing-derived protein isoforms ("spliceoform") ratios also change between fetal and postnatal hearts. Identification of spliceoforms at the protein level remains highly challenging for multiple experimental and data analytical reasons (Blencowe, 2017; Lau et al., 2019; Wang et al., 2018). To overcome the issue of sequence redundancy, i.e., most peptides are no longer unique to any single database entry due to the high degree of sequence similarities between canonical and alternative isoforms, we applied a custom protein rollup method for parsimony. Briefly, peptides shared across two proteins from the same gene are assigned to the canonical form only, unless the alternative isoform possesses one or more uniquely mappable peptides, in which case the iBAQ values of any shared peptides are distributed across the canonical and alternative isoforms proportionally to their iBAQ values from unique peptides. Protein entries identified at FDR < 0.01 under the same root uniprot accessions are then grouped together to compare their proportional abundance as above.

Applying the same cutoff criteria as the paralog pairs (FDR adjusted $P < 0.01$, ≥ 5% minor isoform fraction, absolute log2 fold-change > 0.5), we find 11 pairs of isoform switches between fetal and postnatal hearts (**Figure 3A**). In addition, aiming to identify more splice isoforms, we used a custom RNA-seq guided workflow that is more suitable for uncovering additional peptides (see **methods**). For shared proteins, both workflows measured highly similar protein iBAQ values over >5 orders of magnitude (correlation coefficient: 0.85–0.86) (**Supplemental Figure S2**) with similar numbers of implicated paralog isoform shifts. This workflow recovered 10 of 11 isoform shifts and further uncovered and quantified 5 more isoform

shifts at adjusted P < 0.01, minor isoform fraction > 0.05, and abs(logFC) > 0.5, bringing the total number of protein splice isoform signatures to 16 (**Table 2**).

The data recapitulated a known shift of pyruvate kinase from M2 (PKM) to M1 (PKM2) isoform (n.b. The M2 isoform is designated as canonical on UniProt, hence the M1 isoform's database name is PKM-2) (**Figure 3B**). The M2 isoform differs from M1 by a pair of mutually exclusive exons at exon 9 and exon 10, and is associated with cancer metabolism as well as glucose metabolism in heart failure (Rees et al., 2015). Mammals have four tropomyosin genes TPM1, TPM2, TPM3, and TPM4, and each of them also has splicing-derived isoforms. We observed the shift from TPM2-2 (non-muscle tropomyosin 2.1) to TPM2 (muscle tropomyosin 2.2) (**Figure 3C**)

Other spliceoform shifts include in PDLIM5 (**Figure 3D**) from the canonical toward PDLIM5-3. The UniProt PDLIM5-3 sequence misses AA 98-206 and is 239 aa long compared to 591 aa long of the canonical PDLIM5 sequence. The identified protein therefore likely corresponds to the reported short PDLIM5 isoform that participates in binucleation during cardiac development (Gan et al., 2022). In addition, a splicing change of integrin beta 1 causes a relative expansion of the striated muscle 1D isoform (ITGB1-2) (Belkin et al., 1996, p. 1) over the canonical 1A (ITGB1) isoform (**Figure 3E**). In parallel, mitofilin (IMMT), which forms part of the MICOS complex in the mitochondrial inner membrane, shows a depletion of the uncharacterized-3 isoform in postnatal hearts (**Figure 3F**).

Spliceoform Pair	Canonical Protein Name	logFC	adj.P.Val	MIF	Workflow 1 (SwissProt/ Sage)	Workflow 2 (JCAST /Fragger)
Asph/Asph-2	Aspartyl/asparaginyl beta-hydroxylase (EC 1.14.11.16) (Aspartate beta-hydroxylase) (ASP beta-hydroxylase) (Peptide-aspartate beta-dioxygenase)	2.284	1.08E-09	0.297	✅	✅
Pdlim5/Pdlim5-3	PDZ and LIM domain protein 5 (Enigma homolog) (Enigma-like PDZ and LIM domains protein)	1.966	7.9E-10	0.467	✅	✅
Tpm2/Tpm2-2	Tropomyosin beta chain (Beta-tropomyosin) (Tropomyosin-2)	1.731	5.74E-05	0.169	✅	✅
Pkm/Pkm-2	Pyruvate kinase PKM (EC 2.7.1.40) (Pyruvate kinase muscle isozyme) (Threonine-protein kinase PKM2) (EC 2.7.11.1) (Tyrosine-protein kinase PKM2) (EC 2.7.10.2)	1.447	3.05E-05	0.433	✅	✅
Itgb1/Itgb1-2	Integrin beta-1 (Fibronectin receptor subunit beta) (VLA-4 subunit beta) (CD antigen CD29)	1.436	1.3E-08	0.144	✅	✅
Atp2a2/Atp2a2-2	Sarcoplasmic/endoplasmic reticulum calcium ATPase 2 (SERCA2) (SR Ca(2+)-ATPase 2) (EC 7.2.2.10) (Calcium pump 2) (Calcium-transporting ATPase sarcoplasmic reticulum type, slow twitch skeletal muscle isoform) (Endoplasmic reticulum class 1/2 Ca(2+) ATPase)	1.16	1.35E-05	0.07	✅	✅
Mical2/Mical2-J3	[F-actin]-monooxygenase MICAL2 (EC 1.14.13.225) (ERK2-binding testicular protein 1) (MICAL C-terminal-like protein) (Mical-cL) (Molecule interacting with CasL protein 2) (MICAL-2) (mMical2)	1.158	7.6E-05	0.066	❌	✅
Immt/Immt-3	MICOS complex subunit Mic60 (Mitochondrial inner membrane protein) (Mitofilin)	-0.889	2.77E-05	0.237	✅	✅
Qki/Qki-6	KH domain-containing RNA-binding protein QKI (Protein quaking) (MqkI)	0.849	5.6E-04	0.271	❌	✅
Gls/Gls-2	Glutaminase kidney isoform, mitochondrial (GLS) (EC 3.5.1.2) [Cleaved into: Glutaminase kidney isoform, mitochondrial 68 kDa chain; Glutaminase kidney isoform, mitochondrial 65 kDa chain]	-0.788	0.00168	0.272	✅	✅

Sptbn1/Sptbn1-2	Spectrin beta chain, non-erythrocytic 1 (Beta-II spectrin) (Embryonic liver fodrin) (Fodrin beta chain)	0.761	0.000108	0.211	✅	✅
Set/Set-2	Protein SET (Phosphatase 2A inhibitor I2PP2A) (I-2PP2A) (Template-activating factor I) (TAF-I)	0.753	3.04E-04	0.358	❌	✅
Sorbs1/Sorbs1-3	Sorbin and SH3 domain-containing protein 1 (Ponsin) (SH3 domain protein 5) (SH3P12) (c-Cbl-associated protein) (CAP)	-0.748	1.91E-05	0.296	✅	✅
Fbln1/Fbln1-2	Fibulin-1 (FIBL-1) (Basement-membrane protein 90) (BM-90)	0.651	0.00257	0.418	✅	❌
Golga4/Golga4-J7	Golgin subfamily A member 4 (tGolgin-1)	0.593	2.71E-03	0.097	❌	✅
Sptan1-2/Sptan1-J2	Spectrin alpha chain, non-erythrocytic 1 (Alpha-II spectrin) (Fodrin alpha chain)	0.521	6.95E-03	0.278	❌	✅

Table 2: Spliceoform protein ratios with significant shifts in usage between fetal vs. postnatal hearts. logFC: log2 fold-change expressed in fetal/postnatal hearts. MIF: minor isoform fraction.

With the JCAST/MSFragger workflow, we further identified an isoform shift in QKI (Quaking, KH domain containing RNA binding) (**Figure 3G**); QKI is an RNA-binding protein (RBP) that mediates alternative splicing and is important for cardiomyocyte differentiation as well as implicated in ischemic injury. It itself has three major isoforms QKI-5 (canonical), QKI-6, and QKI-7 with different C-terminus residues. We found an increase in QKI-6 over QKI(-5) ratio in postnatal hearts, which mirrors the decline of QKI-5 seen over embryogenesis in the brain (Larocque et al., 2009). Whereas QKI-5 has a nuclear localization signal and is thought to regulate pre-mRNA splicing; QKI-6 is largely cytoplasmic (Larocque et al., 2009) and may function in RNA stability or post-transcriptional regulations. In the heart, deletion of *QKI* locus led to abrogated cardiomyocyte contractility in hESC that is rescued by canonical QKI or (QKI-5) but not QKI-6, further supporting functional diversification in cardiac cells (Chen et al., 2021). A change in QKI-5 and QKI-6 ratios from the same gene may therefore signify in a change RNA-binding function that together with other known RBP changes in cardiac development (D'Antonio et al., 2022; Gan et al., 2022) can initiate a broad reordering of splicing networks.

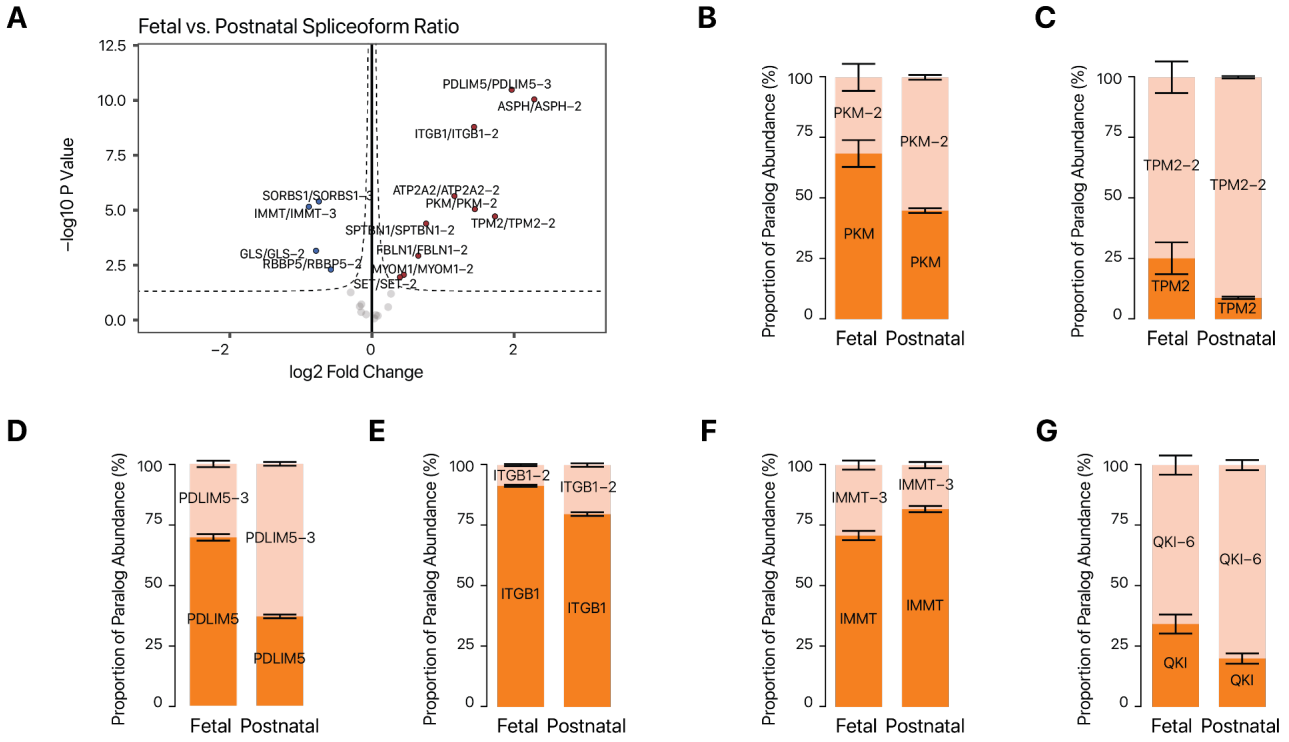

Figure 3. Spliceoform usage in fetal vs. postnatal hearts. **A.** Volcano plot showing the log2 fold-change (x-axis) vs. –log10 P value (y-axis) of spliceoform pairs (n=5 for fetal and postnatal hearts each). **B–G**. Bar charts showing the proportion from 0 to 100% of **B.** PKM (M2) /PKM-2 (M1), **C.** TPM2/TPM2-2, **D.** PDLIM5/PDLIM-3, **E.** ITGB1 (1A)/ITBG1-2 (1D), **F.** IMMT3/IMMT-3, and **G.** QKI (-5)/QKI-6. Selected spliceoform pairs are shown with limma adjusted $P < 0.01$; average minor isoform fraction ≥ 0.05.

Reversal of glycolysis isoform ratios in pathological cardiac remodeling.

Finally, we examined whether some isoform shifts are reversed in cardiac remodeling. To do so, we compared adult and aged mice administered with saline or 20 mg/kg isoproterenol for up to 14 days to induce pathological cardiac hypertrophy. On individual protein and pathway levels, isoproterenol treatment led to an increase in striated muscle contraction proteins and depletion of mitochondrial metabolism and respiratory chain proteins as expected, suggesting the experiments captured the proteomic landscape of pathological hypertrophy (**Supplemental Figure S3**).

As the changes in hypertrophy vs. normal hearts might be expected to be more subtle, we focused on which isoform pairs are significantly different (limma FDR adjusted P value < 0.05) while recapitulating the direction of changes in fetal/postnatal comparisons, regardless of log fold-change. Comparing the isoform ratios in the hypertrophy data set with the fetal/postnatal data, we saw multiple glycolytic proteins that showed significant changes in isoform usage in hypertrophy and partially reverted the direction of the fetal gene profiles. Prominently, this includes a return to a lower LDHB/LDHA ratio (**Figure 4A**). Overexpression of LDHA in neonatal rat ventricular myocytes has been shown to drive hypertrophic cardiac growth in rodent models (Dai et al., 2020), suggesting the possibility that this particular isoform shift may contribute maladaptively to hypertrophy. In addition, we observed a return toward a lower PFKM/PFKP ratio (**Figure 4B**), the latter of which is known to be up-regulated in failing human hearts and may be maladaptive (Vigil-Garcia et al., 2021). Another glycolytic gene, PGAM, shows a return toward a higher PGAM1/PGAM2 ratio (**Figure 4C**).

Additionally, we observed a return toward a lower inorganic phosphatase isoform PPA2/PPA1 ratio (**Figure 4D**), which are important metabolic proteins in the mitochondria but have not been explored in the context of cardiac development or remodeling. There is a return toward a higher EEF1A1/EEF1A2 ratio (**Figure 4E**), two homologous members of the eEF1A component of the eEF1 complex with unclear distinction of function. In addition, one splice isoform (ITGAB) also reversed in isoform usage partially (**Figure 4F**). In each case however, only a partial reversal was observed and moreover, the magnitude of changes in hypertrophy appeared smaller than reported transcript changes, suggesting some buffering at the protein level. Other isoform pairs, including HK1/HK2 were also found to differ in the hypertrophy samples but were not found to be different between fetal and postnatal hearts in this experiment.

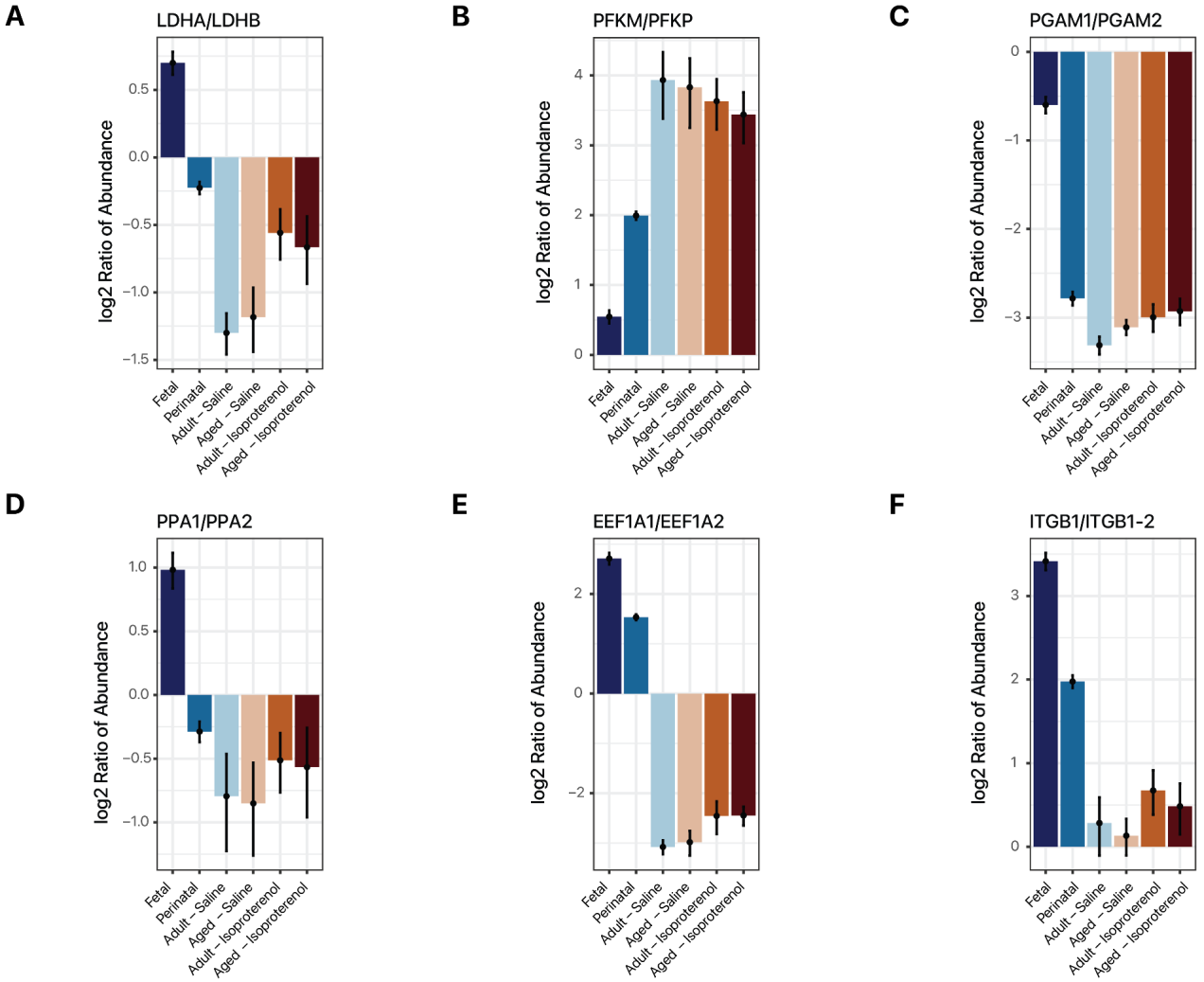

Figure 4. Partial return toward fetal isoform ratios in hypertrophic hearts. **A–F.** Bar charts showing the log2 ratio of abundance (y-axis) in **A.** LDHA/LDHB; **B.** PFKM/PFKP; **C.** PGAM1/PGAM2; **D.** PPA1/PPA2; **E.** EEF1A1/EEF1A2; and **F.** ITGB1/ITGB1-2 splicing in fetal, perinatal, adult normal, aged normal, adult hypertrophy, and aged hypertrophy hearts, showing partial reversion towards fetal characteristic ratios upon hypertrophy. Selected significant proteins are shown with limma FDR adjusted P value < 0.05 in the hypertrophy comparisons (n=4–8 per group) under expression ~ treatment + age + batch. Error bars: s.d. of ratios.

Summary

To our knowledge, this is the first proteomics study to systematically examine the ratiometric changes of isoform pairs in fetal hearts. The proportional abundance of isoforms in isoform groups is relevant to function because fold-change values alone can obscure stark differences in the abundances of two proteins, in a manner analogous to the stoichiometric occupancy of post-translational modification sites vs. fold-change of signals. In some cases, a minor form may be of insufficient quantity to matter functionally, in particular where many non-canonical splice isoforms may be expressed at a low level (e.g., a minor isoform that is 4-fold up-regulated may in reality change from 0.1% to 0.4% of the main isoform). The data discovered new isoforms that to our knowledge have not been implicated in the fetal genetic program in the heart that may be relevant to understanding cardiac development and disease. As only one fetal and one postnatal time point is examined, other isoform shifts likely exist that await exploration. Moreover, as we focused on ratiometric measures between two isoforms here, instances where both isoforms are simultaneously regulated are not within the scope of this study. Fetal genes that are not part of a paralog or spliceoform pairs (e.g., ANF/NPPA) are likewise excluded. The incomplete proteome

coverage of mass spectrometry experiments may preclude some isoforms from being identified. While an arbitrary 5% minor isoform fraction cutoff is used here to define sufficiently abundant isoforms, we are aware that protein isoforms with drastically lower abundance may still be functionally important. In the hypertrophic mouse heart experiment, we find that only some fetal gene shifts are reversed, and moreover the ones that do revert only exhibit partial changes. The relatively low number of samples and limited depth here coupled to variations in the disease model may limit the number of fetal reversals that can be identified.

In summary, we report a proteomics approach to finding ratiometric differences in isoform usage. The data recapitulated hallmark fetal genes and discovered novel candidate shifts, providing a resource of detectable fetal gene isoforms at the protein levels as well as their changes in postnatal hearts.

Methods

Animal Experiments

All animal protocols were approved by the Institutional Animal Care and Use Committee (IACUC) guidelines at the University of Colorado Denver/Anschutz Medical Campus. Fetal heart and postnatal hearts (n=5 each) were acquired commercially at E17.5 and P1 from Zyagen (San Diego, CA), weighed, and homogenized for proteomics profiling (see below). For normal and hypertrophic mouse hearts, wild-type C57BL/6J mice were purchased from Jackson Laboratories (Bar Harbor, ME, USA) and housed in a temperature-controlled environment on a 12-h light/dark cycle and with free access to normal chow diet and water under National Institutes of Health (NIH) guidelines for the Care and Use of Laboratory Animals. Adult (16-17 wk) and aged (86 wk) mice were administered with saline or (dose?) isoproterenol by micro-osmotic pump (ALZET) implantation for a duration of 7 or 14 days (male and female, n = 2 per sex per age group, 32 animals total) as previously described (Lam et al., 2014). The animals were euthanized, followed by measurement of body weight, heart weight and tibia length. Left ventricles were collected and kept frozen at –80 °C.

Protein Chemistry and Mass Spectrometry

Tissue homogenization was performed with a handheld homogenizer (OMNI International). Samples were placed on ice for 1 minute to allow cooling down. Repeat for a total of 3 rounds of homogenization. Homogenized tissues were sonicated with a handheld sonicator (Fisher Model 120), at 40% amplitude for 1 s, pause for 5 s, for 15 cycles. The samples were then centrifuged at 5,000 × g for 1 min at 4°C, and vortex for 10 s, and repeated for three rounds of sonication and centrifugation. The extracted protein samples were further centrifuged at 14,000 × g for 15 min at 4°C to collect supernatants and measure protein concentration with the BCA protein assay kit following manufacturer instructions. The samples were then reduced, alkylated, and digested with sequencing-grade trypsin as previously described (Han et al., 2022). The digested peptides were labeled with TMT 10-plex isobaric tags (Thermo), and fractionated using high-pH reversed-phase columns (Pierce) following manufacturer instructions. Mass spectrometry was performed on a Q-Exactive HF orbitrap high-resolution mass spectrometer (Thermo) coupled to a Thermo Easy-nLC UPLC liquid chromatography system. The LC gradient was as follows: 0 – 105 minutes, 0 – 30% B; 105 – 110 minutes, 30 – 70% B, 110 – 115 minutes: 70 – 100% B; 115 – 120 minutes: hold; at 300 nL/min. Mass spectrometry data were acquired in data dependent acquisition (DDA) mode using typical settings including 60,000 MS1 and MS2 resolution, 3e6 MS1 AGC; 2e5 MS2 AGC; 110 ms maximum IT; 15 TopN; isolation window 0.7 m/z; normalized CE 28, 30, 32; and 30 seconds dynamic exclusion.

Data Analysis and Statistics

Mass spectrometry data was searched using Sage v.0.14.5 (Lazear, 2023) aarch64-apple-darwin build to identify proteins and to measure peptide MS2 TMT and MS1 LFQ (label-free quantification) intensity, using typical settings including: missed_cleavages: 2, precursor_tol: –20 to +20 ppm; fragment_tol: –20 to +20 ppm; isotope: false; static_mods: C 57.0215 K 229.1629; variable mods: M 15.9949 ^ 229.1629 S 229.1629; generate_decoys: true; isotope_errors: 0 – 3; quant: tmt: Tmt10; quant: lfq: true, The database used was retrieved on 2023-09-15 from UniProt (The UniProt Consortium et al., 2023) to contain 25,530

Swiss-Prot *Mus musculus* reviewed canonical and isoform entries. A peptide-level multiple testing adjusted q value cutoff of 0.01 was used for confident identification.

TMT intensity is corrected for isotope spillover using non-negative least squares (Searle and Yergey, 2020). For fetal experiments, TMT values are column sum normalized within each TMT block. A first-pass unique iBAQ value (intensity-based absolute quantification) estimate of the absolute quantity if each protein (Schwanhäusser et al., 2011) was calculated by the sum of MS1 LFQ of all peptides confidently mappable to a unique protein, divided by the protein sequence length. A second-pass distributed iBAQ was then calculated by adding to the unique iBAQ values the proportional iBAQ values of all peptides shared by multiple proteins, divided by the unique iBAQ of the proteins. Protein abundance was then calculated by multiplying the distributed iBAQ to row-normalized TMT values. The protein abundance values were then column sum normalized followed by variance stabilizing transformation for the fetal data with 1 TMT block; an internal reference normalization using two reference channels across each of the 5 TMT blocks was further carried out after column sum normalization for the hypertrophy experiment.

Paralogs are retrieved from Ensembl (Martin et al., 2023) using biomaRt (Durinck et al., 2009), filtering for 50% mean bidirectional gene sequence identity between two paralogs within a pair. Orthology type is retrieved from Ensembl. We then identified all disjoint paralog groups using gene names and calculated the ratios of protein abundance in each sample. The ratios of splice isoforms were calculated similarly in independent comparisons.

To corroborate the protein quantification values and to further identify splicing-derived isoforms, we performed database search using a computational strategy we previously developed to enable RNA-seq-guided proteomics to identify protein isoforms from the mass spectrometry data (Han et al., 2020; Lau et al., 2019). Briefly, a custom database was generated using JCAST v.0.3.4 (Ludwig and Lau, 2021) with deep RNA sequencing data generated from the mouse heart as described (Han et al., 2022). The non-canonical sequences were then appended to the Swiss-Prot canonical + isoform database to yield a total of 29,102 forward entries. This database was used to repeat the database search using MSFragger v.3.8 (Kong et al., 2017) using typical settings, including precursor_mass_lower: –20 ppm; precursor_mass_upper: 20 ppm; fragment_mass_tolerance 20 ppm; isotope error: 0/1/2; allowed_missed_cleavage: 2; num_enzyme_termini: 1. The search results then underwent confidence determination using MSBooster v.1.1.6 (Yang et al., 2023) and Percolator v.3.0 (The et al., 2016). The MS2 and MS1 intensity of confidently identified peptides (Percolator q value <= 0.01) were then extracted using pyTMT v.0.4.1 (Dostal et al., 2020) and Riana v.0.7.1 (Hammond et al., 2022), respectively. Protein abundance for spliceoform pairs was calculated as above.

To perform statistical tests of the isoform ratios, we used limma v.3.58.1 (Ritchie et al., 2015) with a formula of expression ~ age is used for the fetal/postnatal comparison; for hypertrophy: expression ~ treatment + age + block is used . An FDR adjusted limma adjusted P value cutoff of 0.01% is used for fetal comparisons, along with filters by minor isoform fraction, absolute log fold change, and conservation cutoffs as noted in the results. An FDR adjusted limma adjusted P of 0.1 (10% FDR) is used for hypertrophy comparisons. Functional analysis was performed using GSEA against Reactome terms using the ReactomePA package.

Acknowledgments
This work was supported in part by NIH grants R01-HL169473, R01-GM144456, R01-HL141278, R35-GM146815, and R00 HL144829.

Supplemental Figures

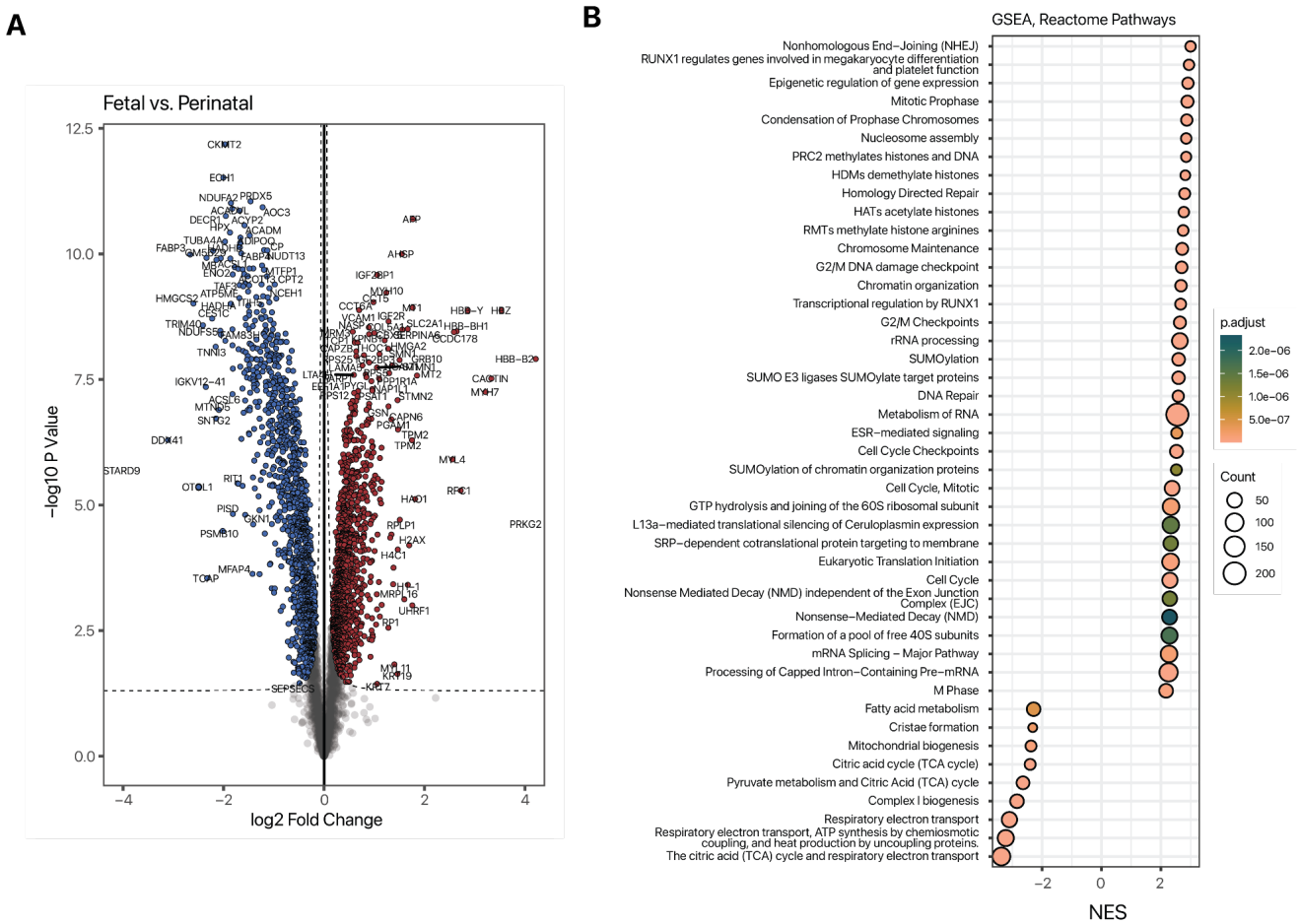

Supplemental Figure S1. Individual protein abundance changes in fetal vs. postnatal hearts. **A.** Volcano plot showing the log2 fold-change (x-axis) vs. –log10 P value (y-axis) of compared individual proteins (fetal/postnatal). **B.** Gene set enrichment analysis (GSEA) of protein fold-change (fetal/postnatal) against Reactome pathways. Color: GSEA adjusted P values; x-axis: GSEA normalized enrichment score (NES); size: number of proteins mapped to pathway.

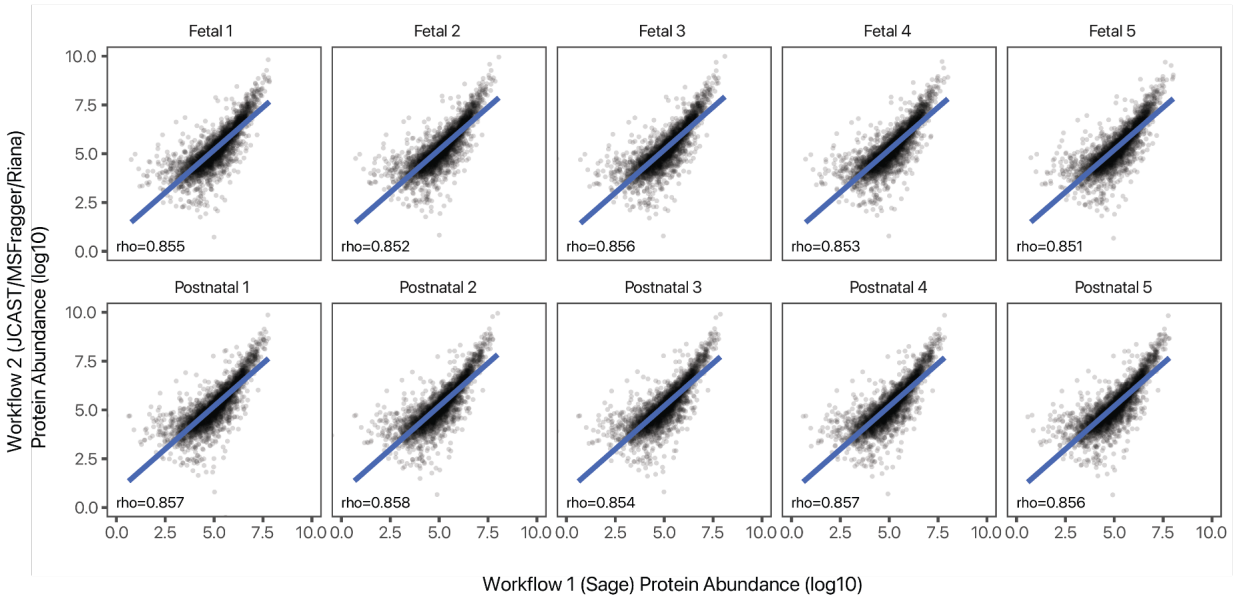

Supplemental Figure S2. Scatter plots showing the measured protein abundance (MS1 and MS2 combined) in (x-axis) the Sage/SwissProt workflow and (y-axis) the JCAST/MSFragger workflow. Robust correlation (Spearman's correlation coefficient rho: 0.851 – 0.858) was observed across ten samples over 5 orders of magnitude in protein abundance in the fetal/postnatal comparisons between the two workflows, despite the use of different search engine, post-processing step, MS1 peak area integration, and TMT intensity extraction tools.

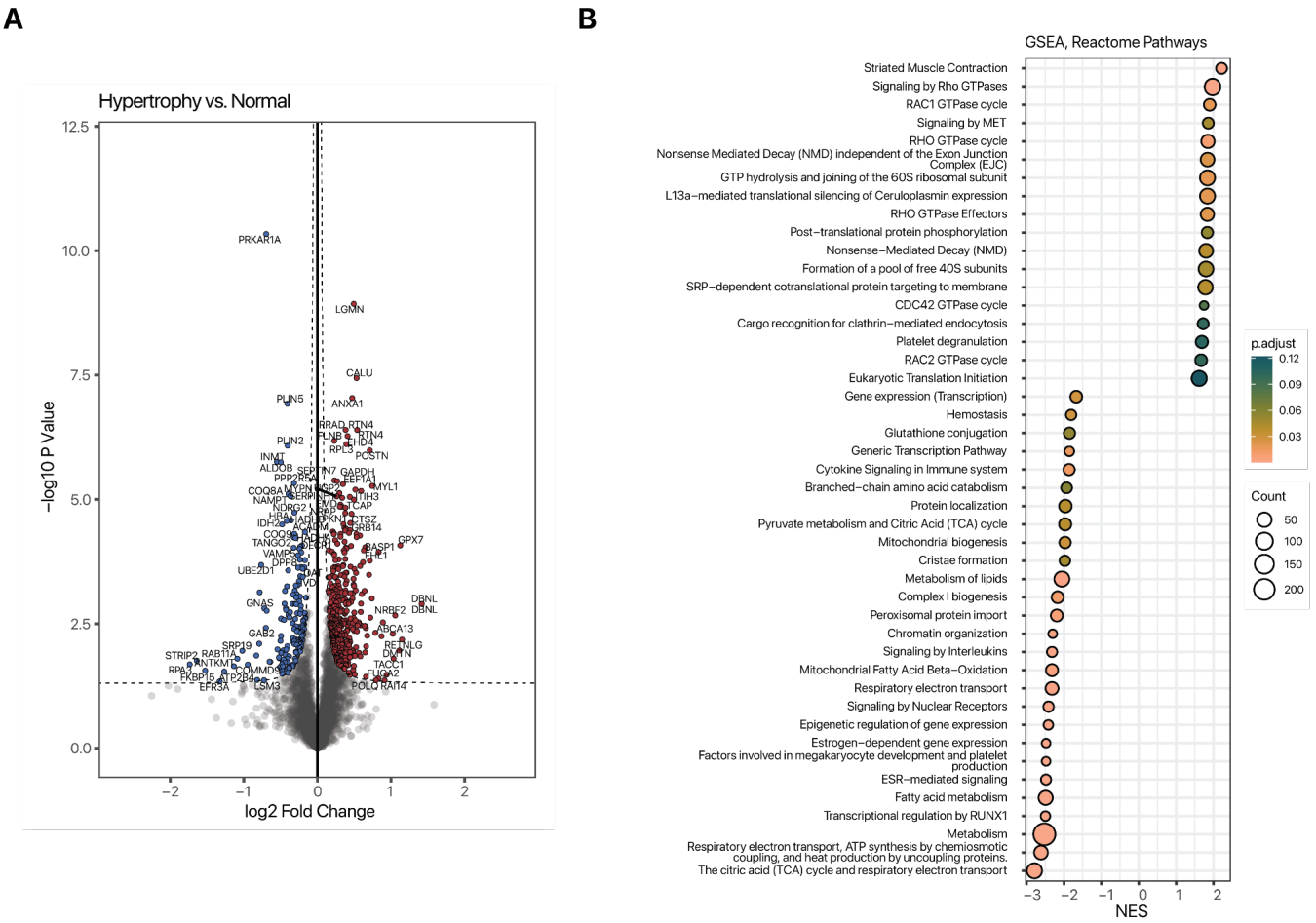

Supplemental Figure S3. Individual protein abundance changes in hypertrophy vs. normal hearts. **A.** Volcano plot showing the log2 fold-change (x-axis) vs. –log10 P value (y-axis) of compared individual proteins (hypertrophy/normal). **B.** Gene set enrichment analysis (GSEA) of protein fold-change (hypertrophy/normal) against Reactome pathways. Color: GSEA adjusted P values; x-axis: GSEA normalized enrichment score (NES); size: number of proteins mapped to pathway. As expected, striated muscle contraction proteins are up-regulated in hypertrophic hearts; mitochondrial proteins are down-regulated.

References

Anflous, K., Armstrong, D.D., Craigen, W.J., 2001. Altered Mitochondrial Sensitivity for ADP and Maintenance of Creatine-stimulated Respiration in Oxidative Striated Muscles from VDAC1-deficient Mice. J. Biol. Chem. 276, 1954–1960. https://doi.org/10.1074/jbc.M006587200

Baines, C.P., Kaiser, R.A., Sheiko, T., Craigen, W.J., Molkentin, J.D., 2007. Voltage-dependent anion channels are dispensable for mitochondrial-dependent cell death. Nat. Cell Biol. 9, 550–555. https://doi.org/10.1038/ncb1575

Belkin, A.M., Zhidkova, N.I., Balzac, F., Altruda, F., Tomatis, D., Maier, A., Tarone, G., Koteliansky, V.E., Burridge, K., 1996. Beta 1D integrin displaces the beta 1A isoform in striated muscles: localization at junctional structures and signaling potential in nonmuscle cells. J. Cell Biol. 132, 211–226. https://doi.org/10.1083/jcb.132.1.211

Bergeron, S.E., Zhu, M., Thiem, S.M., Friderici, K.H., Rubenstein, P.A., 2010. Ion-dependent polymerization differences between mammalian beta- and gamma-nonmuscle actin isoforms. J. Biol. Chem. 285, 16087–16095. https://doi.org/10.1074/jbc.M110.110130

Bhavsar, P.K., Dhoot, G.K., Cumming, D.V., Butler-Browne, G.S., Yacoub, M.H., Barton, P.J., 1991.

Developmental expression of troponin I isoforms in fetal human heart. FEBS Lett. 292, 5–8. https://doi.org/10.1016/0014-5793(91)80820-s

Blencowe, B.J., 2017. The Relationship between Alternative Splicing and Proteomic Complexity. Trends Biochem. Sci. 42, 407–408. https://doi.org/10.1016/j.tibs.2017.04.001

Castelló, A., Rodríguez-Manzaneque, J.C., Camps, M., Pérez-Castillo, A., Testar, X., Palacín, M., Santos, A., Zorzano, A., 1994. Perinatal hypothyroidism impairs the normal transition of GLUT4 and GLUT1 glucose transporters from fetal to neonatal levels in heart and brown adipose tissue. Evidence for tissue-specific regulation of GLUT4 expression by thyroid hormone. J. Biol. Chem. 269, 5905–5912. https://doi.org/10.1016/S0021-9258(17)37547-6

Chen, X., Liu, Ying, Xu, C., Ba, L., Liu, Z., Li, Xiuya, Huang, J., Simpson, E., Gao, H., Cao, D., Sheng, W., Qi, H., Ji, H., Sanderson, M., Cai, C.-L., Li, Xiaohui, Yang, L., Na, J., Yamamura, K., Liu, Yunlong, Huang, G., Shou, W., Sun, N., 2021. QKI is a critical pre-mRNA alternative splicing regulator of cardiac myofibrillogenesis and contractile function. Nat. Commun. 12, 89. https://doi.org/10.1038/s41467-020-20327-5

Cheng, E.H.-Y., Sheiko, T.V., Fisher, J.K., Craigen, W.J., Korsmeyer, S.J., 2003. VDAC2 Inhibits BAK Activation and Mitochondrial Apoptosis. Science 301, 513–517. https://doi.org/10.1126/science.1083995

Dai, C., Li, Q., May, H.I., Li, C., Zhang, G., Sharma, G., Sherry, A.D., Malloy, C.R., Khemtong, C., Zhang, Y., Deng, Y., Gillette, T.G., Xu, J., Scadden, D.T., Wang, Z.V., 2020. Lactate Dehydrogenase A Governs Cardiac Hypertrophic Growth in Response to Hemodynamic Stress. Cell Rep. 32, 108087. https://doi.org/10.1016/j.celrep.2020.108087

D'Antonio, M., Nguyen, J.P., Arthur, T.D., Matsui, H., Donovan, M.K.R., D'Antonio-Chronowska, A., Frazer, K.A., 2022. In heart failure reactivation of RNA-binding proteins is associated with the expression of 1,523 fetal-specific isoforms. PLOS Comput. Biol. 18, e1009918. https://doi.org/10.1371/journal.pcbi.1009918

DeLaughter, D.M., Bick, A.G., Wakimoto, H., McKean, D., Gorham, J.M., Kathiriya, I.S., Hinson, J.T., Homsy, J., Gray, J., Pu, W., Bruneau, B.G., Seidman, J.G., Seidman, C.E., 2016. Single-Cell Resolution of Temporal Gene Expression during Heart Development. Dev. Cell 39, 480–490. https://doi.org/10.1016/j.devcel.2016.10.001

Dirkx, E., Da Costa Martins, P.A., De Windt, L.J., 2013. Regulation of fetal gene expression in heart failure. Biochim. Biophys. Acta BBA - Mol. Basis Dis. 1832, 2414–2424. https://doi.org/10.1016/j.bbadis.2013.07.023

Dostal, V., Wood, S.D., Thomas, C.T., Han, Y., Lau, E., Lam, M.P.Y., 2020. Proteomic signatures of acute oxidative stress response to paraquat in the mouse heart. Sci. Rep. 10, 18440. https://doi.org/10.1038/s41598-020-75505-8

Durinck, S., Spellman, P.T., Birney, E., Huber, W., 2009. Mapping identifiers for the integration of genomic datasets with the R/Bioconductor package biomaRt. Nat. Protoc. 4, 1184–1191. https://doi.org/10.1038/nprot.2009.97

Franco, D., Lamers, W., Moorman, A.F., 1998. Patterns of expression in the developing myocardium: towards a morphologically integrated transcriptional model. Cardiovasc. Res. 38, 25–53. https://doi.org/10.1016/S0008-6363(97)00321-0

Gan, P., Wang, Z., Morales, M.G., Zhang, Y., Bassel-Duby, R., Liu, N., Olson, E.N., 2022. RBPMS is an RNA-binding protein that mediates cardiomyocyte binucleation and cardiovascular development. Dev. Cell 57, 959-973.e7. https://doi.org/10.1016/j.devcel.2022.03.017

Gelens, L., Qian, J., Bollen, M., Saurin, A.T., 2018. The Importance of Kinase–Phosphatase Integration: Lessons from Mitosis. Trends Cell Biol. 28, 6–21. https://doi.org/10.1016/j.tcb.2017.09.005

Gygi, S.P., Rochon, Y., Franza, B.R., Aebersold, R., 1999. Correlation between protein and mRNA abundance in yeast. Mol. Cell. Biol. 19, 1720–1730. https://doi.org/10.1128/MCB.19.3.1720

Hammond, D.E., Simpson, D.M., Franco, C., Wright Muelas, M., Waters, J., Ludwig, R.W., Prescott, M.C., Hurst, J.L., Beynon, R.J., Lau, E., 2022. Harmonizing Labeling and Analytical Strategies to Obtain Protein Turnover Rates in Intact Adult Animals. Mol. Cell. Proteomics 21, 100252. https://doi.org/10.1016/j.mcpro.2022.100252

Han, Y., Wennersten, S.A., Wright, J.M., Ludwig, R.W., Lau, E., Lam, M.P.Y., 2022. Proteogenomics reveals sex-biased aging genes and coordinated splicing in cardiac aging. Am. J. Physiol.-Heart Circ. Physiol. 323, H538–H558. https://doi.org/10.1152/ajpheart.00244.2022

Han, Y., Wright, J.M., Lau, E., Lam, M.P.Y., 2020. Determining Alternative Protein Isoform Expression Using RNA Sequencing and Mass Spectrometry. STAR Protoc. 1, 100138. https://doi.org/10.1016/j.xpro.2020.100138

Kong, A.T., Leprevost, F.V., Avtonomov, D.M., Mellacheruvu, D., Nesvizhskii, A.I., 2017. MSFragger: ultrafast and comprehensive peptide identification in mass spectrometry-based proteomics. Nat. Methods 14, 513–520. https://doi.org/10.1038/nmeth.4256

Lam, M.P.Y., Wang, D., Lau, E., Liem, D.A., Kim, A.K., Ng, D.C.M., Liang, X., Bleakley, B.J., Liu, C., Tabaraki, J.D., Cadeiras, M., Wang, Y., Deng, M.C., Ping, P., 2014. Protein kinetic signatures of the remodeling heart following isoproterenol stimulation. J. Clin. Invest. 124, 1734–1744. https://doi.org/10.1172/JCI73787

Larocque, D., Fragoso, G., Huang, J., Mushynski, W.E., Loignon, M., Richard, S., Almazan, G., 2009. The QKI-6 and QKI-7 RNA Binding Proteins Block Proliferation and Promote Schwann Cell Myelination. PLoS ONE 4, e5867. https://doi.org/10.1371/journal.pone.0005867

Lau, E., Han, Y., Williams, D.R., Thomas, C.T., Shrestha, R., Wu, J.C., Lam, M.P.Y., 2019. Splice-Junction-Based Mapping of Alternative Isoforms in the Human Proteome. Cell Rep. 29, 3751-3765.e5. https://doi.org/10.1016/j.celrep.2019.11.026

Lazear, M.R., 2023. Sage: An Open-Source Tool for Fast Proteomics Searching and Quantification at Scale. J. Proteome Res. 22, 3652–3659. https://doi.org/10.1021/acs.jproteome.3c00486

Lu, Z.Q., Sinha, A., Sharma, P., Kislinger, T., Gramolini, A.O., 2014. Proteomic Analysis of Human Fetal Atria and Ventricle. J. Proteome Res. 13, 5869–5878. https://doi.org/10.1021/pr5007685

Ludwig, R.W., Lau, E., 2021. JCAST: Sample-specific protein isoform databases for mass spectrometry-based proteomics experiments. Softw. Impacts 10, 100163. https://doi.org/10.1016/j.simpa.2021.100163

Martin, F.J., Amode, M.R., Aneja, A., Austine-Orimoloye, O., Azov, A.G., Barnes, I., Becker, A., Bennett, R., Berry, A., Bhai, J., Bhurji, S.K., Bignell, A., Boddu, S., Branco Lins, P.R., Brooks, L., Ramaraju, S.B., Charkhchi, M., Cockburn, A., Da Rin Fiorretto, L., Davidson, C., Dodiya, K., Donaldson, S., El Houdaigui, B., El Naboulsi, T., Fatima, R., Giron, C.G., Genez, T., Ghattaoraya, G.S., Martinez, J.G., Guijarro, C., Hardy, M., Hollis, Z., Hourlier, T., Hunt, T., Kay, M., Kaykala, V., Le, T., Lemos, D., Marques-Coelho, D., Marugán, J.C., Merino, G.A., Mirabueno, L.P., Mushtaq, A., Hossain, S.N., Ogeh, D.N., Sakthivel, M.P., Parker, A., Perry, M., Piližota, I., Prosovetskaia, I., Pérez-Silva, J.G., Salam, A.I.A., Saraiva-Agostinho, N., Schuilenburg, H., Sheppard, D., Sinha, S., Sipos, B., Stark, W., Steed, E., Sukumaran, R., Sumathipala, D., Suner, M.-M., Surapaneni, L., Sutinen, K., Szpak, M., Tricomi, F.F., Urbina-Gómez, D., Veidenberg, A., Walsh, T.A., Walts, B., Wass, E., Willhoft, N., Allen, J., Alvarez-Jarreta, J., Chakiachvili, M., Flint, B., Giorgetti, S., Haggerty, L., Ilsley, G.R., Loveland, J.E., Moore, B., Mudge, J.M., Tate, J., Thybert, D., Trevanion, S.J., Winterbottom, A., Frankish, A., Hunt, S.E., Ruffier, M., Cunningham, F., Dyer, S., Finn, R.D., Howe, K.L., Harrison, P.W., Yates, A.D., Flicek, P., 2023. Ensembl 2023. Nucleic Acids Res. 51, D933–D941. https://doi.org/10.1093/nar/gkac958

Payne, S.H., 2015. The utility of protein and mRNA correlation. Trends Biochem. Sci. 40, 1–3. https://doi.org/10.1016/j.tibs.2014.10.010

Rajabi, M., Kassiotis, C., Razeghi, P., Taegtmeyer, H., 2007. Return to the fetal gene program protects the stressed heart: a strong hypothesis. Heart Fail. Rev. 12, 331–343. https://doi.org/10.1007/s10741-007-9034-1

Read, J.A., Winter, V.J., Eszes, C.M., Sessions, R.B., Brady, R.L., 2001. Structural basis for altered activity of M- and H-isozyme forms of human lactate dehydrogenase. Proteins 43, 175–185. https://doi.org/10.1002/1097-0134(20010501)43:2<175::aid-prot1029>3.0.co;2-#

Rees, M.L., Subramaniam, J., Li, Y., Hamilton, D.J., Frazier, O.H., Taegtmeyer, H., 2015. A PKM2 signature in the failing heart. Biochem. Biophys. Res. Commun. 459, 430–436. https://doi.org/10.1016/j.bbrc.2015.02.122

Reiser, P.J., Portman, M.A., Ning, X.-H., Moravec, C.S., 2001. Human cardiac myosin heavy chain isoforms in fetal and failing adult atria and ventricles. Am. J. Physiol.-Heart Circ. Physiol. 280, H1814–H1820. https://doi.org/10.1152/ajpheart.2001.280.4.H1814

Ritchie, M.E., Phipson, B., Wu, D., Hu, Y., Law, C.W., Shi, W., Smyth, G.K., 2015. limma powers differential expression analyses for RNA-sequencing and microarray studies. Nucleic Acids Res. 43, e47. https://doi.org/10.1093/nar/gkv007

Schwanhäusser, B., Busse, D., Li, N., Dittmar, G., Schuchhardt, J., Wolf, J., Chen, W., Selbach, M., 2011. Global quantification of mammalian gene expression control. Nature 473, 337–342. https://doi.org/10.1038/nature10098

Searle, B.C., Yergey, A.L., 2020. An efficient solution for resolving iTRAQ and TMT channel cross-talk. J. Mass Spectrom. 55, e4354. https://doi.org/10.1002/jms.4354

Srivastava, H., Lippincott, M.J., Currie, J., Canfield, R., Lam, M.P.Y., Lau, E., 2022. Protein prediction models support widespread post-transcriptional regulation of protein abundance by interacting partners. PLOS Comput. Biol. 18, e1010702. https://doi.org/10.1371/journal.pcbi.1010702

Taegtmeyer, H., Sen, S., Vela, D., 2010. Return to the fetal gene program: a suggested metabolic link to gene expression in the heart. Ann. N. Y. Acad. Sci. 1188, 191–198. https://doi.org/10.1111/j.1749-6632.2009.05100.x

The, M., MacCoss, M.J., Noble, W.S., Käll, L., 2016. Fast and Accurate Protein False Discovery Rates on Large-Scale Proteomics Data Sets with Percolator 3.0. J. Am. Soc. Mass Spectrom. 27, 1719–1727. https://doi.org/10.1007/s13361-016-1460-7

The UniProt Consortium, Bateman, A., Martin, M.-J., Orchard, S., Magrane, M., Ahmad, S., Alpi, E., Bowler-Barnett, E.H., Britto, R., Bye-A-Jee, H., Cukura, A., Denny, P., Dogan, T., Ebenezer, T., Fan, J., Garmiri, P., Da Costa Gonzales, L.J., Hatton-Ellis, E., Hussein, A., Ignatchenko, A., Insana, G., Ishtiaq, R., Joshi, V., Jyothi, D., Kandasaamy, S., Lock, A., Luciani, A., Lugaric, M., Luo, J., Lussi, Y., MacDougall, A., Madeira, F., Mahmoudy, M., Mishra, A., Moulang, K., Nightingale, A., Pundir, S., Qi, G., Raj, S., Raposo, P., Rice, D.L., Saidi, R., Santos, R., Speretta, E., Stephenson, J., Totoo, P., Turner, E., Tyagi, N., Vasudev, P., Warner, K., Watkins, X., Zaru, R., Zellner, H., Bridge, A.J., Aimo, L., Argoud-Puy, G., Auchincloss, A.H., Axelsen, K.B., Bansal, P., Baratin, D., Batista Neto, T.M., Blatter, M.-C., Bolleman, J.T., Boutet, E., Breuza, L., Gil, B.C., Casals-Casas, C., Echioukh, K.C., Coudert, E., Cuche, B., De Castro, E., Estreicher, A., Famiglietti, M.L., Feuermann, M., Gasteiger, E., Gaudet, P., Gehant, S., Gerritsen, V., Gos, A., Gruaz, N., Hulo, C., Hyka-Nouspikel, N., Jungo, F., Kerhornou, A., Le Mercier, P., Lieberherr, D., Masson, P., Morgat, A., Muthukrishnan, V., Paesano, S., Pedruzzi, I., Pilbout, S., Pourcel, L., Poux, S., Pozzato, M., Pruess, M., Redaschi, N., Rivoire, C., Sigrist, C.J.A., Sonesson, K., Sundaram, S., Wu, C.H., Arighi, C.N., Arminski, L., Chen, C., Chen, Y., Huang, H., Laiho, K., McGarvey, P., Natale, D.A., Ross, K., Vinayaka, C.R., Wang, Q., Wang, Y., Zhang, J., 2023. UniProt: the Universal Protein Knowledgebase in 2023. Nucleic Acids Res. 51, D523–D531. https://doi.org/10.1093/nar/gkac1052

Thrasher, J.R., Cooper, M.D., Dunaway, G.A., 1981. Developmental changes in heart and muscle phosphofructokinase isozymes. J. Biol. Chem. 256, 7844–7848. https://doi.org/10.1016/S0021-9258(18)43355-8

Vigil-Garcia, M., Demkes, C.J., Eding, J.E.C., Versteeg, D., De Ruiter, H., Perini, I., Kooijman, L., Gladka, M.M., Asselbergs, F.W., Vink, A., Harakalova, M., Bossu, A., Van Veen, T.A.B., Boogerd, C.J., Van Rooij, E., 2021. Gene expression profiling of hypertrophic cardiomyocytes identifies new players in pathological remodelling. Cardiovasc. Res. 117, 1532–1545. https://doi.org/10.1093/cvr/cvaa233

Wang, H., Chen, Y., Li, X., Chen, Guojun, Zhong, L., Chen, Gangbing, Liao, Y., Liao, W., Bin, J., 2016. Genome-wide analysis of alternative splicing during human heart development. Sci. Rep. 6, 35520. https://doi.org/10.1038/srep35520

Wang, X., Codreanu, S.G., Wen, B., Li, K., Chambers, M.C., Liebler, D.C., Zhang, B., 2018. Detection of Proteome Diversity Resulted from Alternative Splicing is Limited by Trypsin Cleavage Specificity. Mol. Cell. Proteomics 17, 422–430. https://doi.org/10.1074/mcp.RA117.000155

Warren, C.F.A., Wong-Brown, M.W., Bowden, N.A., 2019. BCL-2 family isoforms in apoptosis and cancer. Cell Death Dis. 10, 177. https://doi.org/10.1038/s41419-019-1407-6

Yang, K.L., Yu, F., Teo, G.C., Li, K., Demichev, V., Ralser, M., Nesvizhskii, A.I., 2023. MSBooster: improving peptide identification rates using deep learning-based features. Nat. Commun. 14, 4539. https://doi.org/10.1038/s41467-023-40129-9

Yang, M., Petralia, F., Li, Z., Li, H., Ma, W., Song, X., Kim, S., Lee, H., Yu, H., Lee, B., Bae, S., Heo, E., Kaczmarczyk, J., Stępniak, P., Warchoł, M., Yu, T., Calinawan, A.P., Boutros, P.C., Payne, S.H., Reva, B., NCI-CPTAC-DREAM Consortium, Boja, E., Rodriguez, H., Stolovitzky, G., Guan, Y., Kang, J., Wang, P., Fenyö, D., Saez-Rodriguez, J., 2020. Community Assessment of the Predictability of Cancer Protein and Phosphoprotein Levels from Genomics and Transcriptomics. Cell Syst. 11, 186-195.e9. https://doi.org/10.1016/j.cels.2020.06.013

Zannoni, G.F., Monterossi, G., De Stefano, I., Gargini, A., Salerno, M.G., Farulla, I., Travaglia, D., Vellone, V.G., Scambia, G., Gallo, D., 2013. The expression ratios of estrogen receptor α (ERα) to estrogen receptor β1 (ERβ1) and ERα to ERβ2 identify poor clinical outcome in endometrioid endometrial cancer. Hum. Pathol. 44, 1047–1054. https://doi.org/10.1016/j.humpath.2012.09.007

Zhao, Q., Sun, Q., Zhou, L., Liu, K., Jiao, K., 2019. Complex Regulation of Mitochondrial Function During Cardiac Development. J. Am. Heart Assoc. 8, e012731. https://doi.org/10.1161/JAHA.119.012731